Porous In_2O_3 powders prepared by ultrasonic-spray pyrolysis as a NO_2-sensing material: Utilization of polymethylmethacrylate microspheres synthesized by ultrasonic-assisted emulsion polymerization as a template

Takeo Hyodo[1,*], Shu-ichi Furuno[2], Eriko Fujii[1], Katsuhide Matsuo[1], Suguru Motokucho[1], Ken Kojio[1] and Yasuhiro Shimizu[1]

[1]Graduate School of Engineering, Nagasaki University, 1-14 Bunkyo-machi, Nagasaki 852-8521, Japan

[2]Faculty of Engineering, Nagasaki University, 1-14 Bunkyo-machi, Nagasaki 852-8521, Japan

*Corresponding author:

Takeo Hyodo, Dr.

Graduate School of Science and Technology, Nagasaki University

1-14 Bunkyo-machi, Nagasaki 852-8521, Japan

Tel: +81-95-819-2645

Fax: +81-95-819-2643

E-mail: hyodo@nagasaki-u.ac.jp

Abstract

NO_2-sensing properties of porous In_2O_3 (pr-In_2O_3) powders prepared by ultrasonic-spray pyrolysis employing polymethylmethacrylate (PMMA) microspheres as a template has been investigated in this study. The PMMA microspheres were synthesized in water by ultrasonic-assisted emulsion polymerization employing methyl methacrylate monomer, sodium lauryl sulfate as a surfactant and ammonium persulfate as an initiator. The PMMA microspheres synthesized was quite uniform and the particle size was ca. 60.2 nm (measured by dynamic light scattering). The microstructure of pr-In_2O_3 powders prepared was largely dependent on the kind of In_2O_3 sources. The pr-In_2O_3 which was prepared from $In(NO_3)_3$ as an In_2O_3 source (pr-In_2O_3(N)) consisted of submicron-sized spherical particles with well-developed spherical mesopores (several tens of nanometers in pore diameter) and each oxide wall among pores was constructed with meso-sized In_2O_3 particles connected continuously. On the other hand, the pr-In_2O_3 which was prepared from $InCl_3$ as an In_2O_3 source (pr-In_2O_3(Cl)) was composed of a large number of dispersed meso-sized particles and a few submicron-sized dense spherical particles. In contrast, the morphology of conventional In_2O_3 powder (c-In_2O_3) prepared by ultrasonic-spray pyrolysis of PMMA-free $In(NO_3)_3$ aqueous solution as a reference was relatively dense and roughly-spherical with a diameter of ca. 100~700 nm. The responses to 1.0 and 10 ppm NO_2 of pr-In_2O_3 sensors in air were much larger than those of a c-In_2O_3(N) sensor in the temperature range of less than 250°C and 300°C, respectively. In addition, the response and recovery speeds of both the pr-In_2O_3 sensors were much faster than those of the c-In_2O_3(N) sensor, because of the well-developed porous structure of the pr-In_2O_3 sensors.

***Keywords*:** gas sensor; NO_2; porous In_2O_3 powder; ultrasonic-spray pyrolysis; polymethylmethacrylate microsphere; ultrasonic-assisted emulsion polymerization

1. Introduction

Numerous efforts have been directed to strictly controlling the microstructure of gas-sensing materials during the last few decades in order to improve their gas sensitivity and selectivity, because the introduction of well-developed meso- and macro-pores to the gas-sensing materials and their structural optimization are quite effective in controlling their gas reactivity and/or diffusivity [1-7]. In order to improve gas-sensing properties, we also have so far designed microstructural morphology of various gas-sensing materials with different sizes of well-developed pores. For example, mesoporous semiconductor metal oxides (mainly SnO_2 [8-12] and TiO_2 [13, 14]) with large specific surface area and small crystallites were prepared by utilizing a self-assembly of a surfactant such as *n*-cetylpyridinium chloride and a triblock copolymer such as Pluronic P-123 (BASF Corp., $EO_{20}PO_{80}EO_{20}$ (EO: ethylene oxide, PO: propylene oxide)) as a template, and the average diameter of their resultant well-developed mesopores was in the range of 2~5 nm. The treatment of the as-prepared mesoporous oxides with phosphoric acid largely improved their thermal stability at elevated temperatures, while maintainng their large specific surface area (SSA) and small crystallites (CS) (e.g., SSA and CS of typical mesoporous SnO_2 powder: ca. 370 m^2 g^{-1} and 2.0 nm, respectively, even after calcination at 600°C for 5 h [9]). Therefore, the phosphoric-acid treatment enabled us to use mesoporous oxides as gas sensor materials at elevated temperatures. In addition, surface modification of conventional semicondcuting particles with mesoporous SnO_2 layers was also quite effective in enhancing the gas-sensing properties [9, 15, 16].

On the other hand, macroporous oxides [17-26] and carbonates [27, 28] as an gas-sensing material were also prepared by different preparation methods such as modified sol-gel technique [17-20], ultrasonic-spray pyrolysis [21-24], sputtering [25] and pulsed laser deposition [26], employing commercial polymethylmetacrylate (PMMA) microspheres

(150~1500 nm in diameter) as a template. Since the pore size of their macroporous materials was larger than 100 nm in diameter, the introduction of the relatively-large pores improved the gas diffusivity in the gas-sensing films and/or disks significantly, and in turn the gas-sensing properties. However, the pore size was much larger than that enough to improve the gas diffusivity in the gas-sensing mateirals, and the mechanical strength of such materials was also relatively inferior to that of above-mentioned mesoporous materials and conventional gas-sensing materials. Innovative techniques to prepare gas-sensing materials having well-developed middle-sized pores with a diameter of 5~100 nm are absolutely indispensable for designing the nano- and micro-structures suitable for achieving well-controlled gas reactivity and diffusivity in gas-sensing films and/or disks with relatively-high mechanical properties and then for realizing drastic enhancement in the gas-sensing properties.

Therefore, PMMA microspheres with a diameter of several tens nanometer, as a template, were synthesized by ultrasonic-assisted emulsion polymerization and then porous (pr-) In_2O_3 powders were prepared by ultrasonic-spray pyrolysis employing the synthesized PMMA microspheres. Thereafter, their fundamental sensing properties of pr-In_2O_3 sensors to NO_2 in air have been investigated in this study.

2. Experimental

2.1 Synthesis of PMMA microspheres

PMMA microspheres were synthesized by ultrasonic-assisted emulsion polymerization. First, methyl methacrylate monomer (MMA; Wako Pure Chem. Ind., Ltd., 150 cm^3) was washed for three times with 0.05 M NaOH aqueous solution (1 dm^3) to remove a polymerization inhibitor from the MMA monomer. The pure MMA monomer obtained (8 g), sodium lauryl sulfate (SLS; Nacalai Tesque, Inc., 0.1 g) as a surfactant and ammonium

persulfate (Wako Pure Chem. Ind., 0.3 g) as an initiator were added to deionized water (100 cm^3), and then the resultant aqueous solution was ultrasonic-treated by an ultrasonic homogenizer (Nissei Corp., US-150T, 19.5 ± 1 kHz). The polymerization of MMA to PMMA was initiated in the emulsion just upon the irradiation of strong ultrasonic wave to the solution at room temperature (RT), and the solution temerature increased from RT to ca. 60°C within 15 min. After the ultrasonic irradiation for 50 min and subsequent agitation by general blade (400 rpm) at 60°C for 6 h, the stable and uniform dispersion of PMMA microspheres was prepared.

2.2 Preparation of pr-In_2O_3 powders by ultrasonic spray pyrolysis

The PMMA dispersion obtained was mixed with a 0.5 M $In(NO_3)_3$ or $InCl_3$ aqueous solution (PMMA dispension : $In(NO_3)_3$ or $InCl_3$ aqueous solution = 37.5 : 100 in volume ratio) and the mixtures were served as precursor solution of pr-In_2O_3. Figure 1 shows shcematic drawing of a feeding system of the precursor solution atomaized by ultrasonication. The mist of the precursor solution obtained was generated by ultrasonic irradiation (2.4 MHz) and then it was directly heat-treated in an electric furnace at 1100°C under air flowing (2.5 dm^3 min^{-1}) by using a feeding system, as shown in Fig. 1. The porous powders prepared from a 0.5 M $In(NO_3)_3$ and $InCl_3$ aqueous solution were denoted as pr-In_2O_3(N) and pr-In_2O_3(Cl) powders, respectively. A conventional In_2O_3 (c-In_2O_3) powder was also prepared by the similar preparation technique using $In(NO_3)_3$ aqueous solution mixing without the PMMA dispersion [24].

2.3 Characterization of PMMA microspheres and In_2O_3 powders

Thermal decomposition behavior of PMMA microspheres synthesized in this study and commercial PMMA microspheres (Soken Chem. & Eng. Co. Ltd., MP-1451 (ca. 150 nm in

diameter)) was investigated by thermogravimetric and differential thermal analysis (TG-DTA; Shimadzu Co., Ltd., DTG-50) up to 1000°C at a heating rate of 10°C min^{-1}. The particle size distribution of the PMMA microspheres obtained was measured at 25°C by dynamic light scattering (DLS; Malvern instrument Ltd., HPPS). The microstructure of the PMMA and In_2O_3 microspheres was observed by scanning electron microscopy (SEM; JEOL Ltd., JSM-7500F) and transmission electron microscopy (TEM; JEOL Ltd., JEM2010). The pore size distribution and specific surface area (SSA) of the In_2O_3 powders were measured by Barrett-Joyner-Halenda (BJH) and Brunauer-Emmett-Teller (BET) methods using a N_2 adsorption-desorption isotherm (Micromeritics Instrument Corp., Tristar3000), respectively. Crystal phase of the In_2O_3 powders was characterized by X-ray diffraction analysis (XRD; Rigaku Corp., RINT2200) using Cu Kα radiation (40 kV, 40 mA), and their crystallite size (CS) was calculated from the (222) diffraction peak using Scherrer equation.

2.4 Fabrication of thick film sensors and measurement of their gas sensing properties

Thick film sensors were fabricated by screen-printing employing the paste of each In_2O_3 powder on an alumina substrates equipped with a pair of interdigitated Pt electrodes (gap size: ca. 200 μm), followed by calcination at 550°C for 5 h. Gas response of these sensors was measured to 1.0 ppm and 10 ppm NO_2 balanced with air in a flow apparatus at 150~500°C. The magnitude of response to NO_2 was defined as the ratio (R_g/R_a) of sensor resistance after 10 min in NO_2 (R_g) balanced with air to that in air (R_a).

3. Results and Discussions

3.1 Characterizations of PMMA microspheres and In_2O_3 powders

Figure 2 shows TG-DTA profiles of PMMA microspheres synthesized in this study, together with those of commercial PMMA microspheres. The PMMA microspheres

synthesized in this study showed a large exothermic peak at ca. 377°C due to its thermal decomposition, and the temperature is almost comparable to that of the commercial PMMA microspheres (ca. 366°C). The information indicates that the synthesized PMMA microspheres were sufficiently polymerized to a level as is observed for the commercial PMMA microspheres. The magnitude of the exothermic peak of the synthesized PMMA microspheres was much sharper and larger than that of the commercial PMMA microspheres, and this may reflect the difference in the sample mass subjected to TG-DTA measurements. The weight of the commercial PMMA microspheres steeply decreased with a rise in temperature in the range of ca. 200~382°C. On the other hand, the weight of PMMA microspheres synthesized in this study slightly decreased with a rise in temperature in the range of RT ~ ca. 200°C, probably due to the evaporation of water adsorbed. Beyond that the weight largely decreased with a rise in temperature up to 386°C, but the maximum rate of weight loss (slope of the TG curve) of the PMMA microspheres synthesized in this study was slower than that of the commercial PMMA microspheres, probably due to simultaneous decomposition of the SLS residues in this temperature range.

Figure 3 shows particle-size distribution of the PMMA microspheres synthesized in this study. It was found that the average diameter of the PMMA microspheres was ca. 60.2 nm and the PMMA microspheres synthesized were relatively mono-dispersed in the water containing SLS. In addition, it was confirmed that the average diameter of PMMA microspheres synthesized at almost the same conditions was reproducibly in the range of 56~66 nm. Figure 4 shows TEM photographs of the PMMA microspheres which were filtered from the PMMA dispersion. Morphology of all the PMMA microspheres was clearly spherical and uniform, and the average diameter of the PMMA microspheres, which was estimated from Fig. 4, was ca. 61.3 nm. This value was almost comparable to that estimated by the DLS. The results shown in Figs. 2~4 indicate that uniform PMMA

microspheres with a diameter of less than 100 nm were easily synthesized by the ultrasonic-assisted emulsion polymerization, as we had expected, and the size of the PMMA microspheres synthesized was much smaller than that of the smallest one which was employed as a template in our previous study (commercial PMMA microspheres, diameter: ca. 150 nm) [21-25].

Figure 5 shows XRD patterns of pr-In_2O_3 and c-In_2O_3(N) powders. Most peaks of their XRD patterns were assigned to those for the cubic structure of In_2O_3 (JCPDF: 6-416). The crystallite size (CS) of the pr-In_2O_3 powders (17.8 nm for pr-In_2O_3(N) and 15.3 nm for pr-In_2O_3(Cl)), which was calculated by using Scherrer equation, was smaller than that of the c-In_2O_3(N) powder (25.9 nm). PMMA microspheres covered with SLS in the precursor solution may inhibit the crystallite growth of In_2O_3. Figure 6 shows N_2 adsorption-desorption isotherms of pr-In_2O_3 and c-In_2O_3(N) powders, their pore-size distributions which were obtained by BJH method using a N_2 desorption isotherm, together with their specific surface area (SSA), which was calculated by BET method using the N_2 adsorption isotherm. All powders showed hysteresis behavior, especially at a higher relative pressure, and the volume of N_2 adsorped on the c-In_2O_3(N) powder was much smaller than that on the pr-In_2O_3 powders. Therefore, the c-In_2O_3(N) powder showed small pore volume and small SSA (1.56 m^2 g^{-1}), and pore volume and SSA of both the pr-In_2O_3 powders were much larger than that of the c-In_2O_3(N) powder. In addition, the difference of raw chemicals ($In(NO_3)_3$ or $InCl_3$) also affected the the N_2 adsorption-desorption behavior and thus the pore-size distributions were markedly different between pr-In_2O_3(N) and pr-In_2O_3(Cl) powders. Namely, the pr-In_2O_3(N) powder had well-developed pores mainly in the diameter range of 10~100 nm (central pore diameter: ca. 30 nm), while the pr-In_2O_3(Cl) powder had well-developed pores in the diameter less than 10 nm. As a result, the SSA of the pr-In_2O_3(Cl) powder (30.5 m^2 g^{-1}) was larger than that of the pr-In_2O_3(N) powder (19.1 m^2

g^{-1}).

Microstructure of pr-In_2O_3 and c-In_2O_3(N) powders was investigated by SEM and TEM. Figure 7 shows SEM photographs of pr-In_2O_3 and c-In_2O_3(N) powders. Figures 8, 9 and 10 show TEM photographs of pr-In_2O_3 and c-In_2O_3(N) powders, respectively. Morphology of the c-In_2O_3(N) powder was roughly-spherical with ca. 100~700 nm in diameter, and the TEM observation indicated that the bulk was relatively dense. Assuming that the density of In_2O_3 crystal is 7.180 g cm^{-3} [29] and the morphology of the c-In_2O_3(N) powder is spherical and dense perfectly, the geometric size which is estimated from the SSA (1.56 m^2 g^{-1}) is ca. 536 nm in diameter, which almost corresponds on those observed by SEM (Fig. 7(c)) and TEM (Fig. 10). This fact supports that the bulk of the c-In_2O_3(N) powder was almost dense with less pores and consisted of many crystallites (ca. 7.2 x 10^3 or ca. 2.5 x 10^6 crystallites per one spherical particle with a diameter of 100 or 700 nm, respectively, which were estimated from the CS value of ca. 25.9 nm).

On the other hand, morphology of the pr-In_2O_3 powders was quite promising as gas-sensing materials, compared with that of the c-In_2O_3(N) powder. The pr-In_2O_3(N) powder consisted of submicron-sized spherical particles with well-developed spherical mesopores (pore diameter: several tens of nanometers) and a small number of macropores (pore diameter: ca. 100 nm) on the spherical surface as shown in Figs. 7 (a) and 8, and the size of mesopores was quite comparable to that which was estimated by BJH method using a N_2 desorption isotherm (see Fig. 6(a)). The formation of well-developed pores in the internal region of all particles with various sizes was also confirmed by the TEM observation (Fig. 8).

The well-developed mesopores with a diameter of several tens of nanometers seemed to reflect the morphology of the PMMA microspheres in the precursor solution, but the pore size indicated a large shrinkage of voids originating from the PMMA microspheres with a diameter of ca. 60 nm and the morphology of the pores was different from original spherical

shape of PMMA microspheres, probably due to the abrupt and simultenous decomposition of oxide precursors and PMMA microspheres in precursor mists at elevated temperatures and successive sintering of In_2O_3 crystallites. In addition, each oxide wall among the pores were constructed with meso-sized primary particles connected continuously (i.e., crystallites partially sintered each other), as shown in Fig. 8(c). The size of the primary particles which was confirmed from TEM photographs was roughly comparable to the CS value estimated from the XRD spectrum (Fig. 5(a)), but it was not uniform and was distributed in the range of 15~40 nm. The nanopores with a diameter of less than 10 nm, which were confirmed in Fig. 6(b), seem to be formed among such primary particles.

On the other hand, the morphology of the pr-In_2O_3(Cl) powder was quite different from that of the pr-In_2O_3(N) powder, although the difference in the preparation method was only raw chemicals ($InCl_3$ or $In(NO_3)_3$). The pr-In_2O_3(Cl) powder consisted of many meso-sized particles with a diameter of less than 30 nm and a few submicron-sized dense spherical particles, as shown in Figs. 7(b) and 9. It was confirmed that the dense spherical particles consisted of the meso-sized particles as shown in Fig. 9 (b-i). The non-uniform diameter of meso-sized particles (ca. 15~40 nm) was almost similar to those of the pr-In_2O_3(N) powder, and it was also roughly comparable to the CS value estimated from the XRD pattern (Fig. 5(b)). In addition, they were in the form of small agglomerates consisting of a few meso-sized particles partially sintered each other. This microstructure of the pr-In_2O_3(Cl) powder resulted in small pore volume in the diameter range of 10~100 nm and large pore volume in the diameter range of less than 10 nm (see Fig. 6(b)), and the well-developed pores with a diameter of less than 10 nm provides relatively large SSA (30.5 $m^2\ g^{-1}$) in comparison with that of the pr-In_2O_3(N) powder (19.1 $m^2\ g^{-1}$), while the CS value of the pr-In_2O_3(Cl) powder was slightly smaller than that of the pr-In_2O_3(N) powder (see Fig. 5).

These results show that the PMMA microspheres synthesized by this ultrasonic-assisted

polymerization technique can be effectively utilized as a template to prepare attractive gas-sensing materials with well-developed porous structure, small CS and large SSA. In addition, we have confirmed that their microstructure was hardly affected by the post annealing at elevated temperature for gas-sensor fabrication (550°C) for 5 h.

3.2 NO_2-sensing properties of pr-In_2O_3 and c-In_2O_3(N) sensors

Figure 11 shows SEM photographs of cross-section of pr-In_2O_3 and c-In_2O_3(N) sensors. Many spherical particles with different diameters (ca. 0.2~2.0 μm) shown in Figs. 7(a) and 8 were stacked in the pr-In_2O_3(N) layer, while meso-sized particles shown in Figs. 7(b) and 9 accumulated in the pr-In_2O_3(Cl) layer uniformly. The thickness of the pr-In_2O_3(N) layer (ca. 8.9 μm) was comparable to that of the pr-In_2O_3(Cl) layer (ca. 8.6 μm). The c-In_2O_3(N) layer consisted of spherical particles with different diameters (ca. 0.2~1.0 μm) shown in Fig. 7(c) and 10. The thickness of the c-In_2O_3(N) layer (5~6 μm) was thinner than those of the pr-In_2O_3 layers, while the roughness of the c-In_2O_3(N) layer was relatively large than those of the pr-In_2O_3 layers. The thickness and roughness of the oxide layers were not exactly the same among all the sensors, but these differences can be considered within an allowance for valid comparisons of the NO_2-sensing properties of all the sensors and surveys on the microstructural effects of pr-In_2O_3 and c-In_2O_3(N) powders on the sensing properties.

Figure 12 shows response transients of pr-In_2O_3 and c-In_2O_3(N) sensors to NO_2 (1.0 and 10 ppm) balanced with air at 200~400°C. Figures 13 and 14 show operating temperature dependence of response to NO_2 (1.0 and 10 ppm), and response and recovery times of pr-In_2O_3 and c-In_2O_3(N) sensors in air, respectively. The resistance of the c-In_2O_3(N) sensor was much larger than those of the pr-In_2O_3 sensors in the whole temperature range, as shown in Fig. 12. The magnitude of responses to both 1.0 ppm and 10 ppm NO_2 of the pr-In_2O_3 sensors was extremely large at lower temperatures, but it decreased monotonically with an

increase in the operating temperature. In addition, the magnitude of NO_2 responses were hardly dependent on the morphological difference between pr-In_2O_3(N) and pr-In_2O_3(Cl) . The magnitude of response to 10 ppm NO_2 of the c-In_2O_3(N) sensor was comparable to those of the pr-In_2O_3 sensors at higher temperatures (over 300°C), while the c-In_2O_3(N) sensor showed much lower response to 10 ppm NO_2 than those of the pr-In_2O_3 sensors at lower temperature (below 300°C). However, the magnitude of response to low concentration of NO_2 (1.0 ppm) of the c-In_2O_3(N) sensor was larger than those of of the pr-In_2O_3 sensors at higher temperatures (over 300°C), since the magnitude of the response to NO_2 of the c-In_2O_3(N) sensor showed weak NO_2 concentration dependence in the whole temperature range studied. Gurlo et al. have reported that the magnitude of NO_2 response (R_g/R_a) of In_2O_3 powders prepared by a sol-gel method and subsequent heat-treatment at elevated temperatures increased with an increase in the grain size measured by TEM in the grain-size range of 5~100 nm and the In_2O_3 powder with a grain size of ca. 20 nm showed the medium response (R_g/R_a to 1 ppm NO_2: 10~20 at 150°C) among all sensors in air with 50% relative humidity (RH) [30-32]. Thereafter, different In_2O_3 powders, such as porous In_2O_3 microspheres prepared by hydrothremal treatment (CS: 25 nm, R_g/R_a to 10 ppm NO_2: ca. 8 at 250°C in air with 40~50%RH) [33] and In_2O_3 nanoribbons prepared by electrospinning (CS: 18 nm, R_g/R_a to 10 ppm NO_2: ca. 60 at 200°C in air with 40~50%RH) [34], have so far investigated as an attractive NO_2-sensing material. Irrespective of the presence or absence of humidity in the measurment atmosphere and the difference in sensor structure employed (e.g., thickness of oxide layer), it was confirmed that the pr-In_2O_3 sensors fabricated in this study showed relatively large response to NO_2 in comparison with the above-referenced sensors fabricated with In_2O_3 powders with almost the same CS.

On the other hand, response and recovery speeds of the pr-In_2O_3 sensors were much faster than those of the c-In_2O_3(N) sensor in the whole temperature range studied (Fig. 14), owing to

the well-developed porous structure of the pr-In_2O_3 sensors. In addition, the pr-In_2O_3(N) sensor tended to show faster response and recovery speeds than those of the pr-In_2O_3(Cl) sensor. Well-developed large pores with a diameter of 10~100 nm in the pr-In_2O_3(N) powder may improve the gas diffusivity in the sensing layer.

As mentioned above, it is confirmed that the addition of PMMA microspheres to the precursor solution and then the intorduction of porous structure in the In_2O_3 powders were effective in improving the NO_2 response especially at low temperatures and the response and recovery speeds in the whole temperature range studied. The results of the present study predicts the improvement of gas sensing performance of various semiconductor metal oxides other than In_2O_3, by the introduction of nano- and micro-porous strucuture into the powder. The effects of pore size in In_2O_3 powders on the gas-sensing properties are now under investigation.

4. Conclusion

The dispersion containing PMMA microspheres was synthesized by ultrasonic-assisted emulsion polymerization employing the emulsion polymerization employing MMA monomer, SLS as a surfactant and ammonium persulfate as an initiator. Thereafter, pr-In_2O_3 powders were prepared by ultrasonic-spray pyrolysis of $In(NO_3)_3$ or $InCl_3$ aqueous solution containing the synthesized PMMA microspheres as a template. The average diameter of the uniform PMMA microspheres synthesized, which was measured by DLS, was ca. 60.2 nm. The pr-In_2O_3(N) powder consisted of submicron-sized spherical particles with well-developed pores (several tens of nanometers in diameter), while the pr-In_2O_3(Cl) powder was composed of a large number of meso-sized particles with a diameter of less than 30 nm and a few submicron-sized dense spherical particles. On the other hand, the morphology of c-In_2O_3(N) prepared by ultrasonic-spray pyrolysis of PMMA-free $In(NO_3)_3$ aqueous solution as a

reference was roughly spherical with a diameter of ca. 100~700 nm and the bulk was relatively dense. The NO_2 response of pr-In_2O_3 sensors was much larger than that of a c-In_2O_3(N) sensor at lower temperatures. In addition, the response and recovery speeds of the pr-In_2O_3 sensors were much faster than those of the c-In_2O_3(N) sensor, because of the well-developed porous structure of the pr-In_2O_3 sensors.

References

1. R.W.J. Scott, S.M. Yang, G. Chabanis, N. Coombs, D.E. Williams, G.A. Ozin, Tin dioxide opals and inverted opals: near-ideal microstructures for gas sensor, Adv. Mater., 13 (2001) 1468–1472.
2. T. Sasahara, A. Kido, H. Ishihara, T. Sunayama, M. Egashira, Highly sensitive detection of volatile organic compounds by an adsorption/combustion-type sensor based on mesoporous silica, Sens. Actuators B, 108 (2005) 478-483.
3. M. Tiemann, Porous metal oxides as gas sensors, Chem. Eur. J., 13 (2007) 8376-8388.
4. T. Wagner, T. Sauerwald, C.-D. Kohl, T. Waitz, C. Weidmann, M. Tiemann, Gas sensor based on ordered mesoporous In_2O_3, Thin Solid Films, 517 (2009) 6170-6175.
5. J.-H. Lee**,** Gas sensors using hierarchical and hollow oxide nanostructures: overview, Sens. Actuators B, 140 (2009) 319-336.
6. D. Klaus, M. Tiemann, T. Wagner, Nanostructured metal oxides for high-temperature gas sensing: structural stabilization in porous metal oxides, Proc. The 14th Intern. Meeting on Chemical Sensors, May 20-23, Nuremberg, Germany (2012) 1264-1266.
7. Y. Qin, F. Wang, W. Shen, M. Hu, Mesoporous three-dimensional network of crystalline WO_3 nanowires for gas sensing application, J. Alloys and Compounds, in press.
8. T. Hyodo, N. Nishida, Y. Shimizu, M. Egashira, Preparation and gas-sensing properties of thermally stable mesoporous SnO_2, Sens. Actuators B, 83 (2002) 209-215.
9. T. Hyodo, S. Abe, Y. Shimizu, M. Egashira, Gas-sensing properties of ordered mesoporous SnO_2 and effects of coatings thereof, Sens. Actuators B 93 (2003) 590-600.
10. M. Hayashi, T. Hyodo, Y. Shimizu, M. Egashira, Effects of microstructure of mesoporous SnO_2 powders on their H_2 sensing properties, Sens. Actuators B 141 (2009) 465-470.
11. Y. Shimizu, A. Jono, T. Hyodo, M. Egashira, Preparation of large mesoporous SnO_2 powder for gas sensor application, Sens. Actuators B 108 (2005) 56-61.

12. T. Hyodo, K. Murayama, Y. Shimizu, M. Egashira, Large Mesoporous Tin Dioxide Powders for Gas Sensor Materials -Effects of various additives on the mesostructure and the H_2 sensing properties-, Rare Metal Mater. & Eng. 35, Suppl. 3 (2006) 455-458.
13. G. S. Devi, T. Hyodo, Y. Shimizu, M. Egashira, Synthesis of mesoporous TiO_2-based powders and their gas-sensing properties, Sens. Actuators B 87 (2002) 122-129.
14. C. Yu, T. Hyodo, Y. Shimizu, M. Egashira, Preparation of thermally stable mesoporous TiO_2 powder and its gas sensor application, Electrochemistry 71 (2003) 475-480.
15. T. Hyodo, Y. Mitsuyasu, Y. Shimizu, M. Egashira, H_2 and NOx sensing properties of ZnO and In_2O_3 powders modified with mesoporous SnO_2, J. Ceram. Soc. Jpn. 112 (2004) S540-545.
16. Y. Shimizu, K. Tsumura, T. Hyodo, M. Egashira, Effect of simultaneous modification with metal loading and mesoporous layer on H_2 sensing properties of SnO_2 thick film sensors, IEEJ Trans. SM 125 (2005) 70-74.
17. T. Hyodo, K. Sasahara, Y. Shimizu, M. Egashira, Preparation of macroporous SnO_2 films using PMMA microspheres and their sensing properties to NOx and H_2, Sens. Actuators B 106, (2005) 580-590.
18. Y. Takakura, T. Hyodo, Y. Shiimizu, M. Egashira, Preparation of macroporous Eu-doped oxide thick films and their application to gas sensor materials, IEEJ Trans. SM 128 (2008) 137-140.
19. S. Nonaka, T. Hyodo, Y. Shiimizu, M. Egashira, Preparation of macroporous semiconductor gas sensors and their odor sensing properties, IEEJ Trans. SM 128 (2008) 141-144.
20. C. Ishibashi, T. Hyodo, Y. Shimizu, M. Egashira, H_2S sensing properties of macroporous In_2O_3-based sensors, Sensor Lett., 9 (2011) 369-373.
21. K. Hieda, T. Hyodo, Y. Shimizu, M. Egashira, Preparation of porous tin dioxide powder

by ultrasonic spray pyrolysis and their application to sensor materials, Sens. Actuators B 133 (2008) 144-150.

22. M. Hashimoto, H. Inoue, T. Hyodo, Y. Shimizu, M. Egashira, Preparation and gas sensor application of ceramic particles with submicron-size spherical macropores, Sensor Lett. 6 (2008) 887-890.
23. A. Anaraki Firooz, T. Hyodo, A. R. Mahjoub, A. A. Khodadadi, Y. Shimizu, Synthesis of nano- and meso-porous MoO_3-doped SnO_2 as a selective gas-sensing material to NO_2, Sens. Actuators B 147 (2010) 554-560.
24. T. Hyodo, H. Inoue, H. Motomura, K. Matsuo, T. Hashishin, J. Tamaki, Y. Shimizu, M. Egashira, NO_2 sensing properties of macroporous In_2O_3-based powders fabricated by utilizing ultrasonic spray pyrolysis employing polymethylmethacrylate microspheres as a template, Sens. Actuators B 151 (2010) 265-273.
25. T. Hyodo, A. Bieberle-Hütter, J. L. Hertz, H. L. Tuller, Three dimensional arrays of hollow gadolinia-doped ceria microspheres prepared by r.f. magnetron sputtering employing PMMA microsphere templates, J. Electroceram. 17 (2006) 695-699.
26. I.-D. Kim, A. Rothschild, T. Hyodo, H. L. Tuller, Microsphere templating as means of enhancing surface activity and gas sensitivity of $CaCu_3Ti_4O_{12}$ thin films, Nano Lett. 6 (2006) 193 -198.
27. H. Seh, T. Hyodo, H. L. Tuller, Bulk Acoustic Wave Resonator as a sensing platform for NOx at high temperatures, Sens. Actuators B 108, (2005) 547-552.
28. M. Morio, T. Hyodo, Y. Shiimizu, M. Egashira, Effect of macrostructural control of an auxiliary layer on the CO_2 sensing properties of NASICON-based gas sensors, Sens. Actuators B 139 (2009) 563-569.
29. The Merck Index, 14th Ed., Ed. by M. J. O'Neil, Merck & Co., Inc., p. 860 (2006).
30. A. Gurlo, M. Ivanovskaya, N. Bârsan, M. Schweizer-Berberich, U. Weimar, W. Göpel, A.

Diégues, Grain size control in nanocrystalline In_2O_3 semiconductor gas sensors, Sens. Actuators B 44 (1997) 327-333.

31. A. Gurlo, N. Bârsan, M. Ivanovskaya, U. Weimar, W. Göpel, In_2O_3 and MoO_3-In_2O_3 thin film semiconductor gas sensors: interaction with NO_2 and O_3, Sens. Actuators B 47 (1998) 92-99.
32. M. Ivanovskaya, A. Gurlo, P. Bogdanov, Mechanism of O_3 and NO_2 detection and selectivity of In_2O_3 sensors, Sens. Actuators B 77 (2001) 264-267.
33. Z. Cheng, L. Song, X. Ren, Q. Zheng, J. Xu, Novel lotus root slice-like self-assembled In_2O_3 microspheres: synthesis and NO_2-sensing properties, Sens. Actuators B, in print.
34. P. S. Khiabani, A. Hosseinmardi, E. Marzbanred, S. Ghashghaie, C. Zamani, M. Keyanpour-Rad, B. Raissi, NO_2 gas sensor fabrication through AC electrophoretic deposition from electrospun In_2O_3 nanoribbons, Sens. Actuators B 162 (2012) 102-107.

Biographies

Takeo Hyodo received his B. Eng. Degree in applied chemistry and M. Eng. Degree in materials science and technology in 1992 and 1994, respectively, and Dr. Eng. Degree in 1997 from Kyushu University. He has been an assosiate professor at Nagasaki University since 2007. His research interests are the developments of electrochemical devices such as chemical sensors and lithium batteries, and mesoporous and macroporous materials.

Shuichi Furuno received his B. Eng. Degree in materials science and engineering from Nagasaki Uniersity in 2011.

Eriko Fujii received his B. Eng. Degree in materials science and engineering from Nagasaki Uniersity in 2012, and is now a graduate student in graduate school of engineering, Nagasaki University.

Katsuhide Matsuo has been a technical staff at Nagasaki Uniersity since 1971.

Suguru Motokucho received the BS degree and the MS degree in 1997 and 1999 in Engineering from Miyazaki University, respectively, and the PhD degree in 2002 from Tokyo Institute of Technology. He has been an assistant professor at Nagasaki University since 2007. His research interests include polymer synthesis and polymer degradation by utilization of carbon dioxide.

Ken Kojio has been an Associate Professor of Chemistry and Materials Science at the Graduate School of Engineering, Nagasaki University in Japan since 2004, following his work as an Assistant Professor in 2002. He received his BS (1995) and PhD (1999) from the Materials Physics and Chemistry Department, Kyushu University, Japan. His research interests include development of polyelectrolyte for lithiumion batteries, mechanical properties of thermoplastic elastomers and interfacial properties of polymer thin films.

Yasuhiro Shimizu received his B. Eng. Degree in applied chemistry in 1980 and Dr. Eng. Degree in 1987 from Kyushu University. He has been a professor at Nagasaki University since 2005. His current research concentrates on development of odor sensors and design of intelligent sensors by controlling gas diffusivity and reactivity.

Figure Captions

Fig. 1. Schematic drawing of a feeding system of a precursor solution atomized by ultrasonication (2.4 MHz).

Fig. 2. TG-DTA profiles of PMMA microspheres synthesized in this study and commercial PMMA microspheres.

Fig. 3. Particle-size distribution of PMMA microspheres synthesized in this study.

Fig. 4. TEM photographs of the PMMA microspheres synthesized in this study.

Fig. 5. XRD patterns of pr-In_2O_3 and c-In_2O_3(N) powders.

Fig. 6. N_2 adsorption-desorption isotherms and pore-size distributions of pr-In_2O_3 and c-In_2O_3(N) powders.

Fig. 7. SEM photographs of pr-In_2O_3 and c-In_2O_3(N) powders.

Fig. 8. TEM photographs of pr-In_2O_3(N) powder.

Fig. 9. TEM photographs of pr-In_2O_3(Cl) powder. Inserted photograph (b-i): a photograph after improvement in contrast of figure (b).

Fig. 10. TEM photographs of c-In_2O_3(N) powder.

Fig. 11. SEM photographs of cross-section of pr-In_2O_3 and c-In_2O_3(N) sensors.

Fig. 12. Response transients of pr-In_2O_3 and c-In_2O_3(N) sensors to 1.0 ppm and 10 ppm NO_2 balanced with air at 200, 300 and 400°C.

Fig. 13. Operating temperature dependence of response to 1.0 ppm and 10 ppm NO_2 of pr-In_2O_3 and c-In_2O_3(N) sensors in air.

Fig. 14. Operating temperature dependence of response and recovery times of pr-In_2O_3 and c-In_2O_3(N) sensors. Open symbols mean 70% response time or 50% recovery time, and closed symbols mean 90% response time or 90% recovery time. pr-In_2O_3(N) sensor: ○ and ●, pr-In_2O_3(Cl) sensor: □ and ■, c-In_2O_3(N) sensor: △ and ▲.

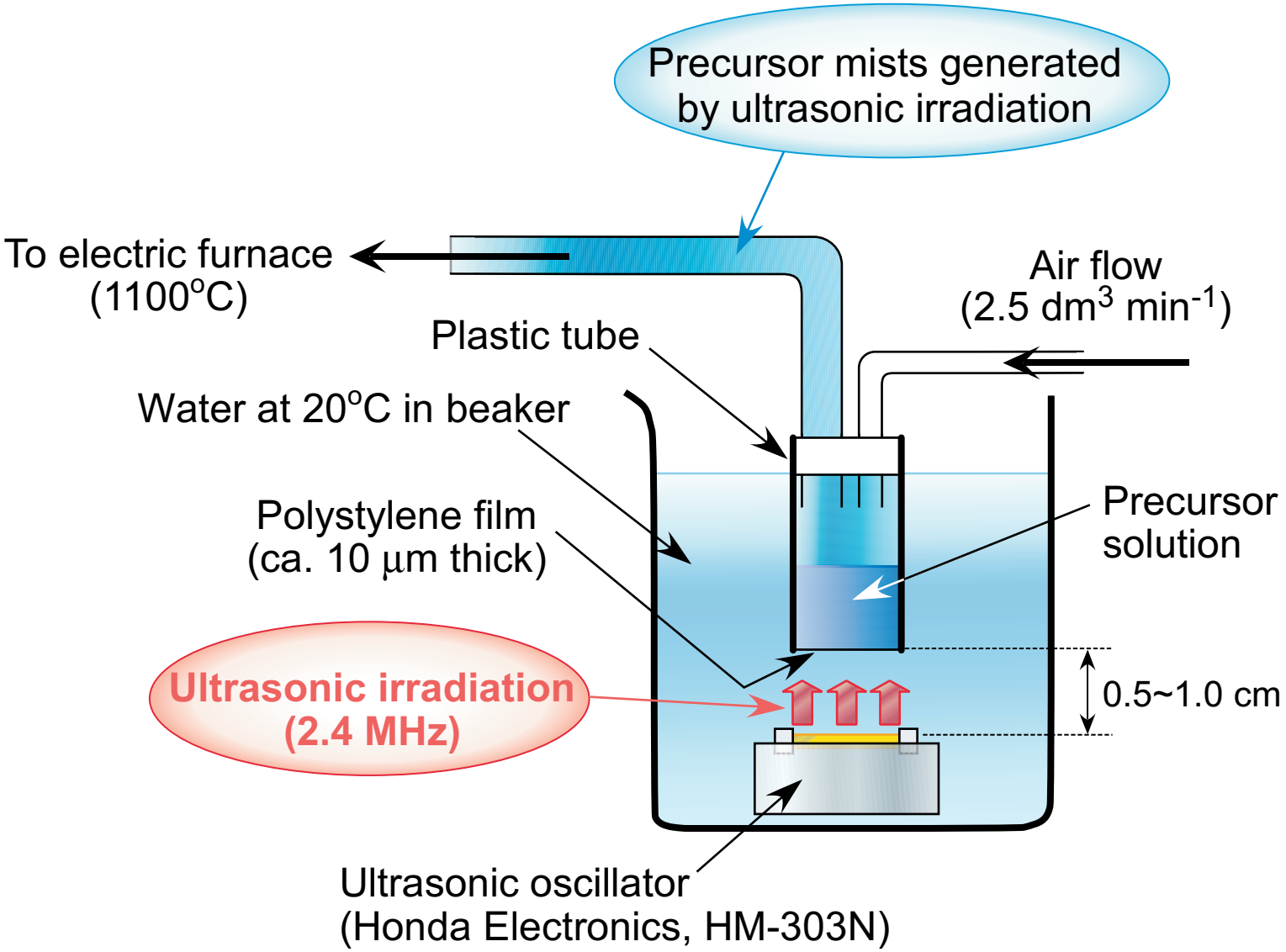

Fig. 1. Hyodo et al.

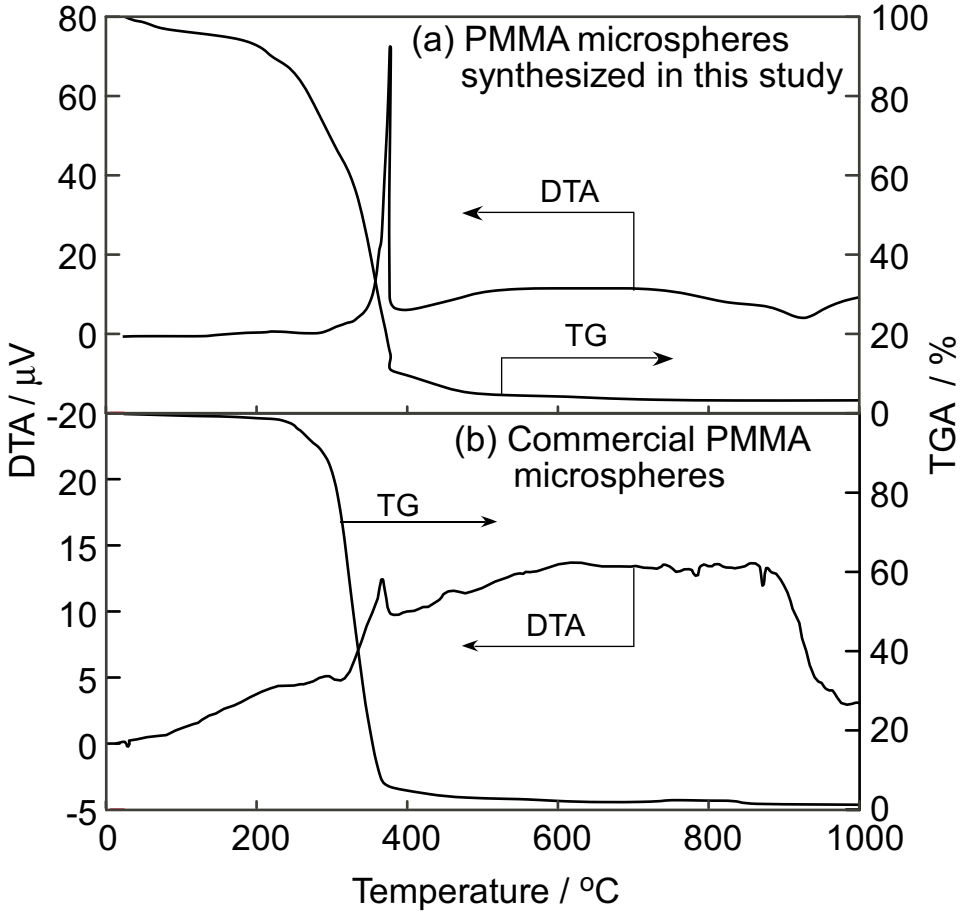

Fig. 2. Hyodo et al.

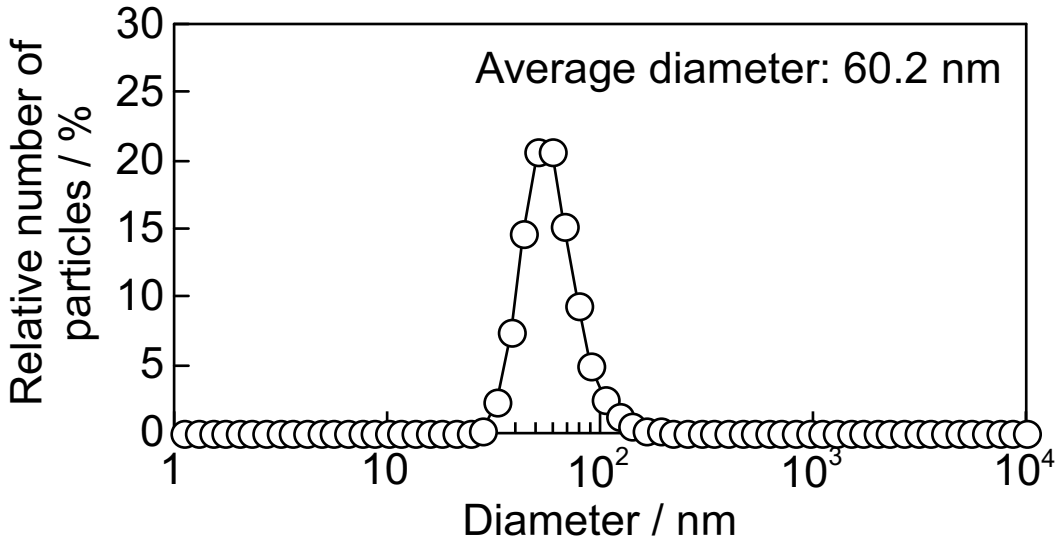

Fig. 3. Hyodo et al.

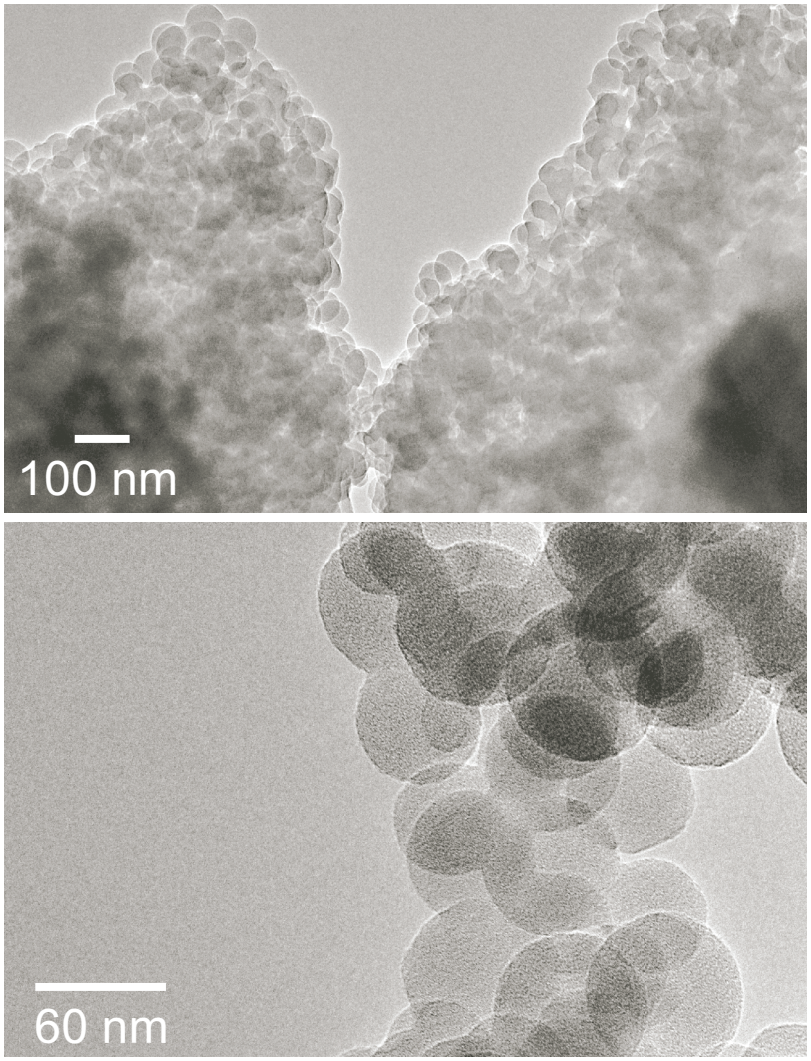

Fig. 4. Hyodo et al.

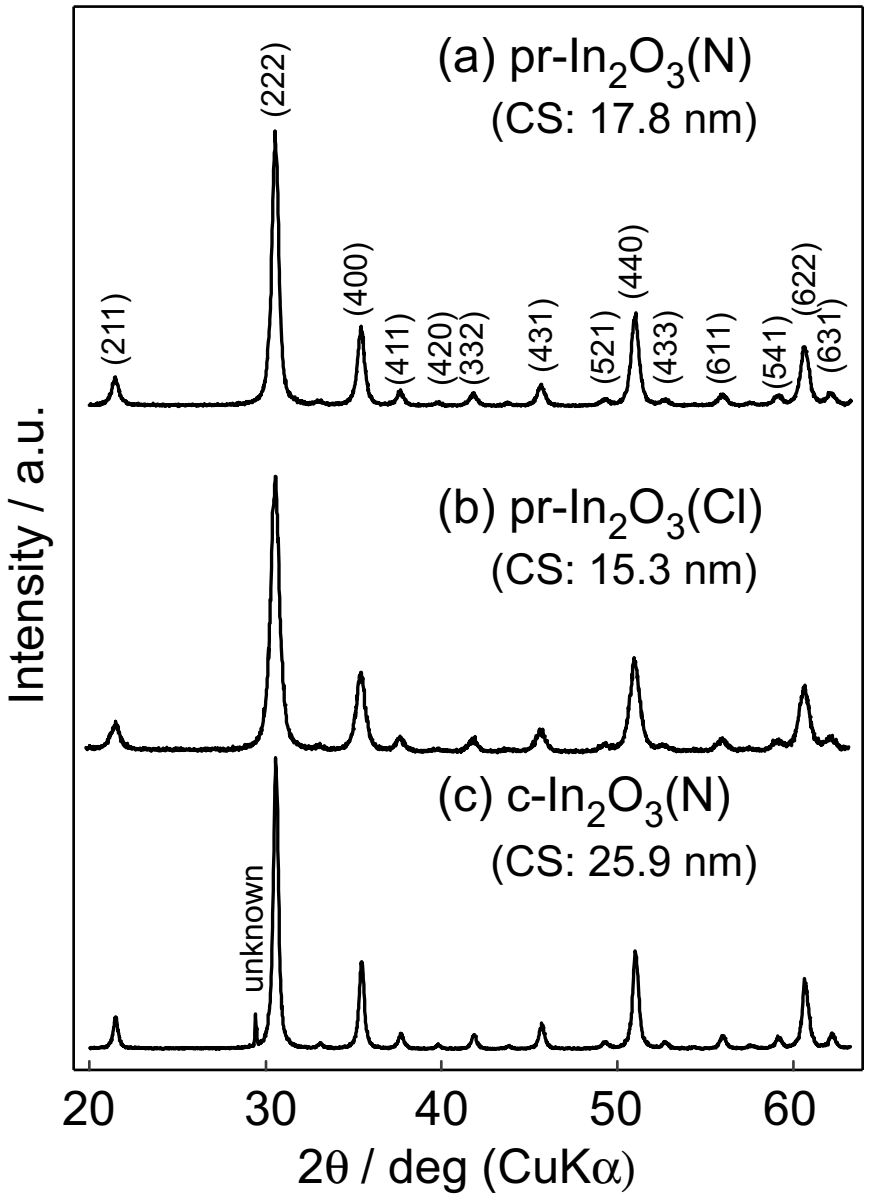

Fig. 5. Hyodo et al.

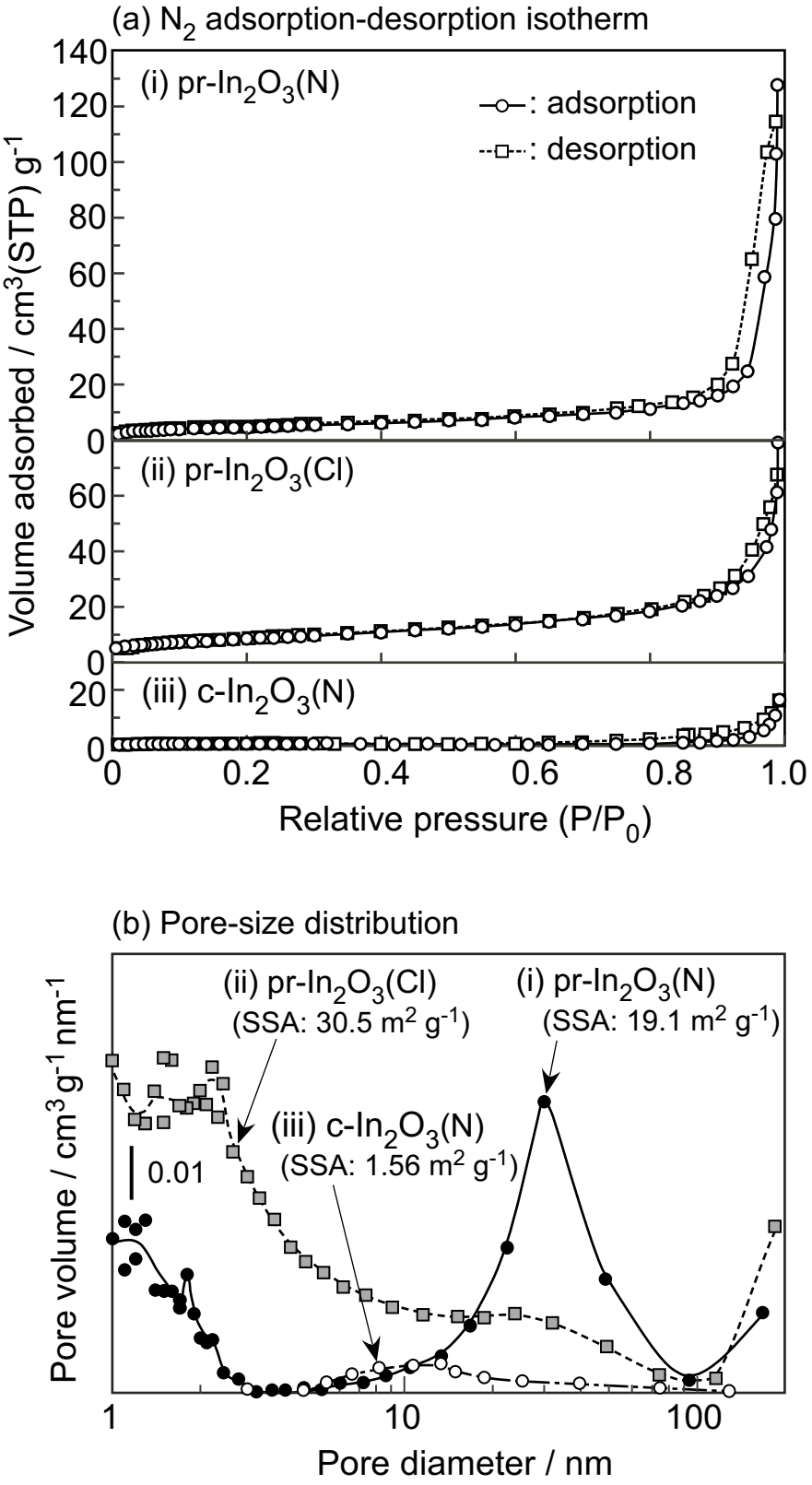

Fig. 6. Hyodo et al.

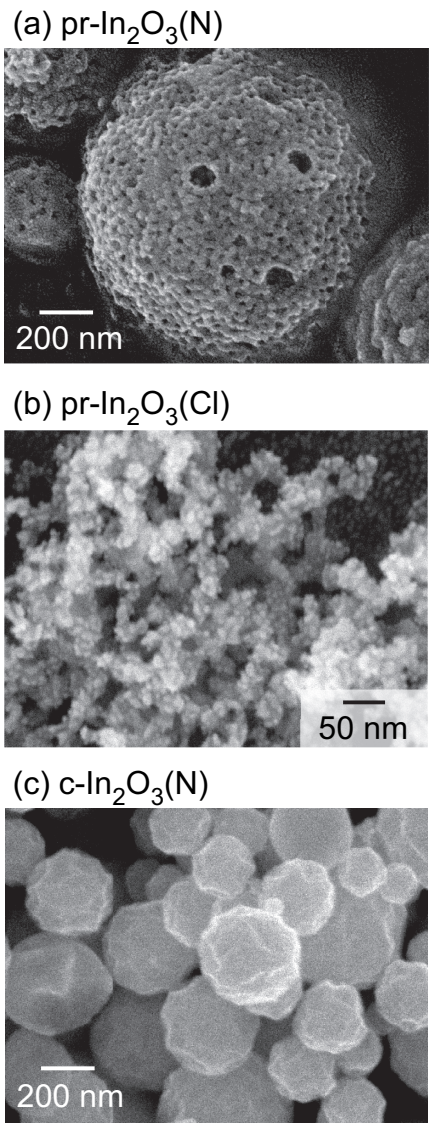

Fig. 7. Hyodo et al.

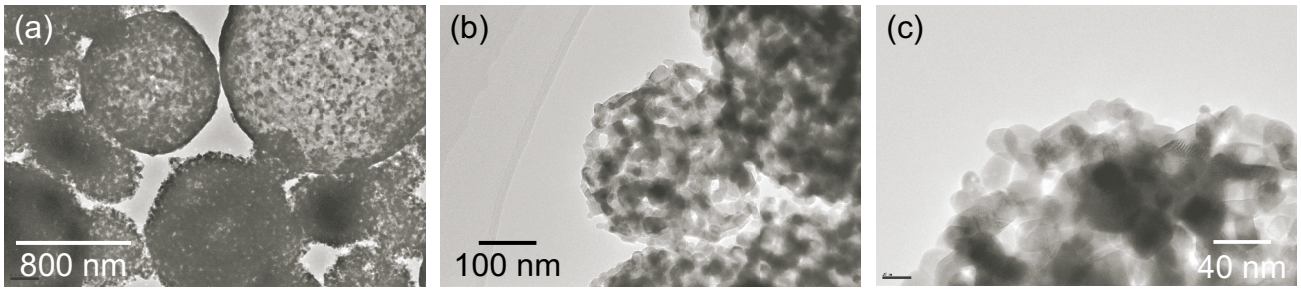

Fig. 8. Hyodo et al.

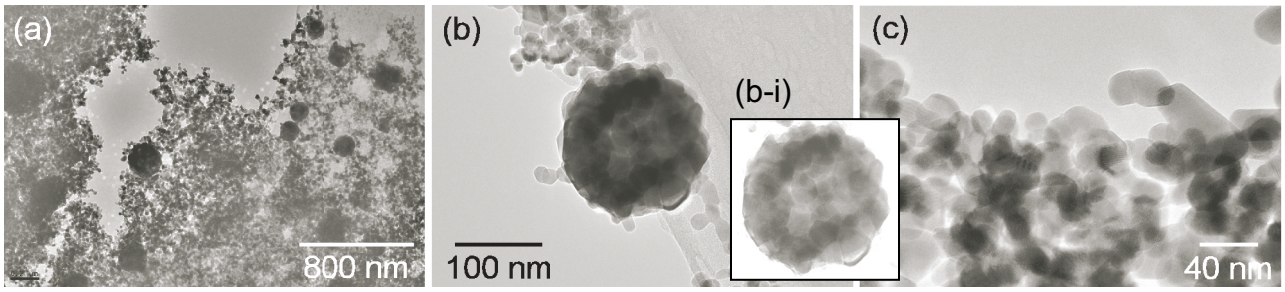

Fig. 9. Hyodo et al.

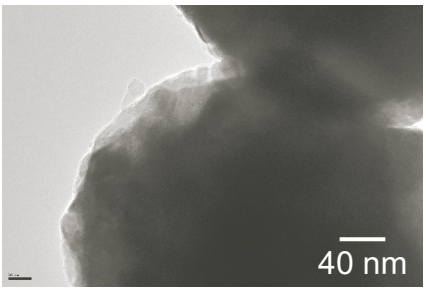

Fig. 10. Hyodo et al.

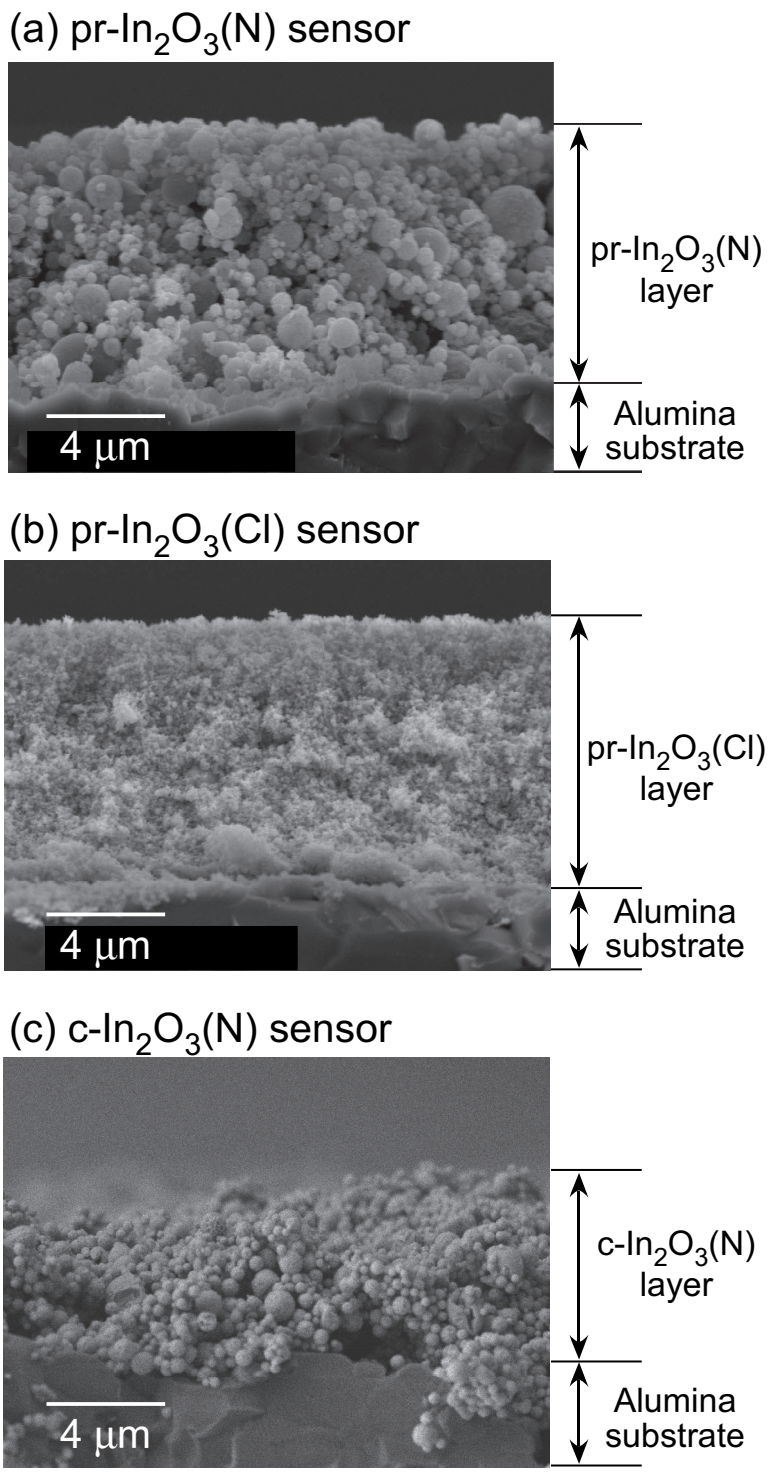

Fig. 11. Hyodo et al.

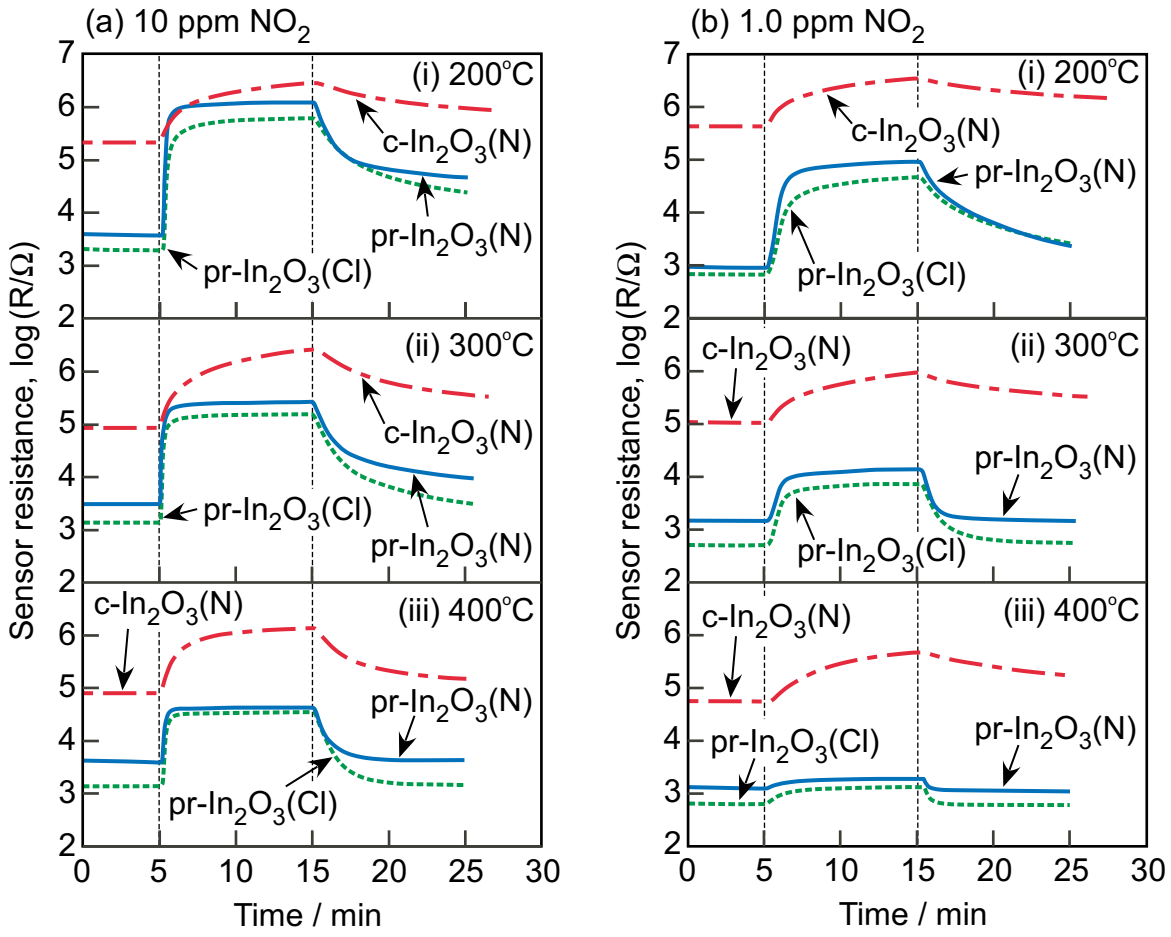

Fig. 12. Hyodo et al.

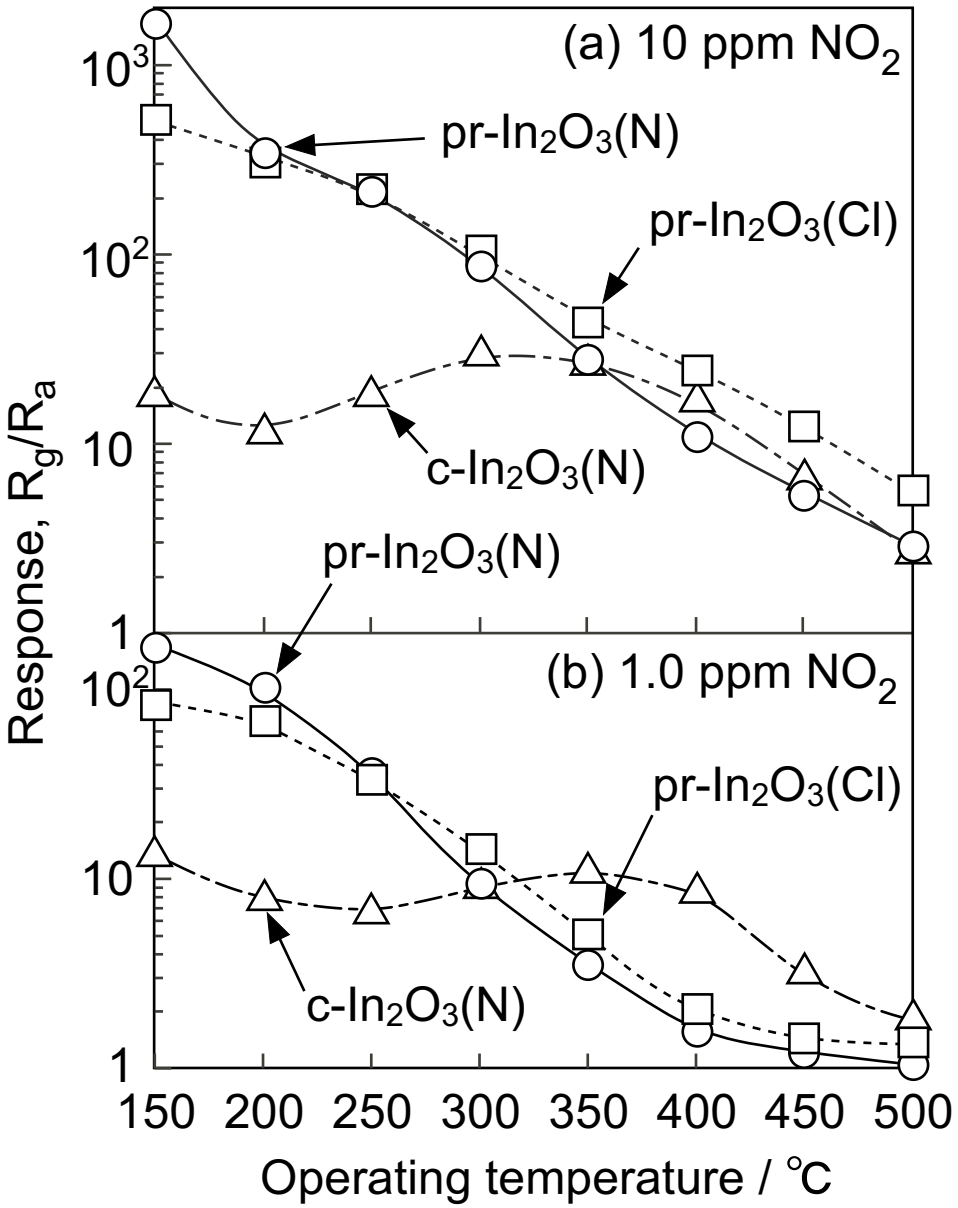

Fig. 13. Hyodo et al.

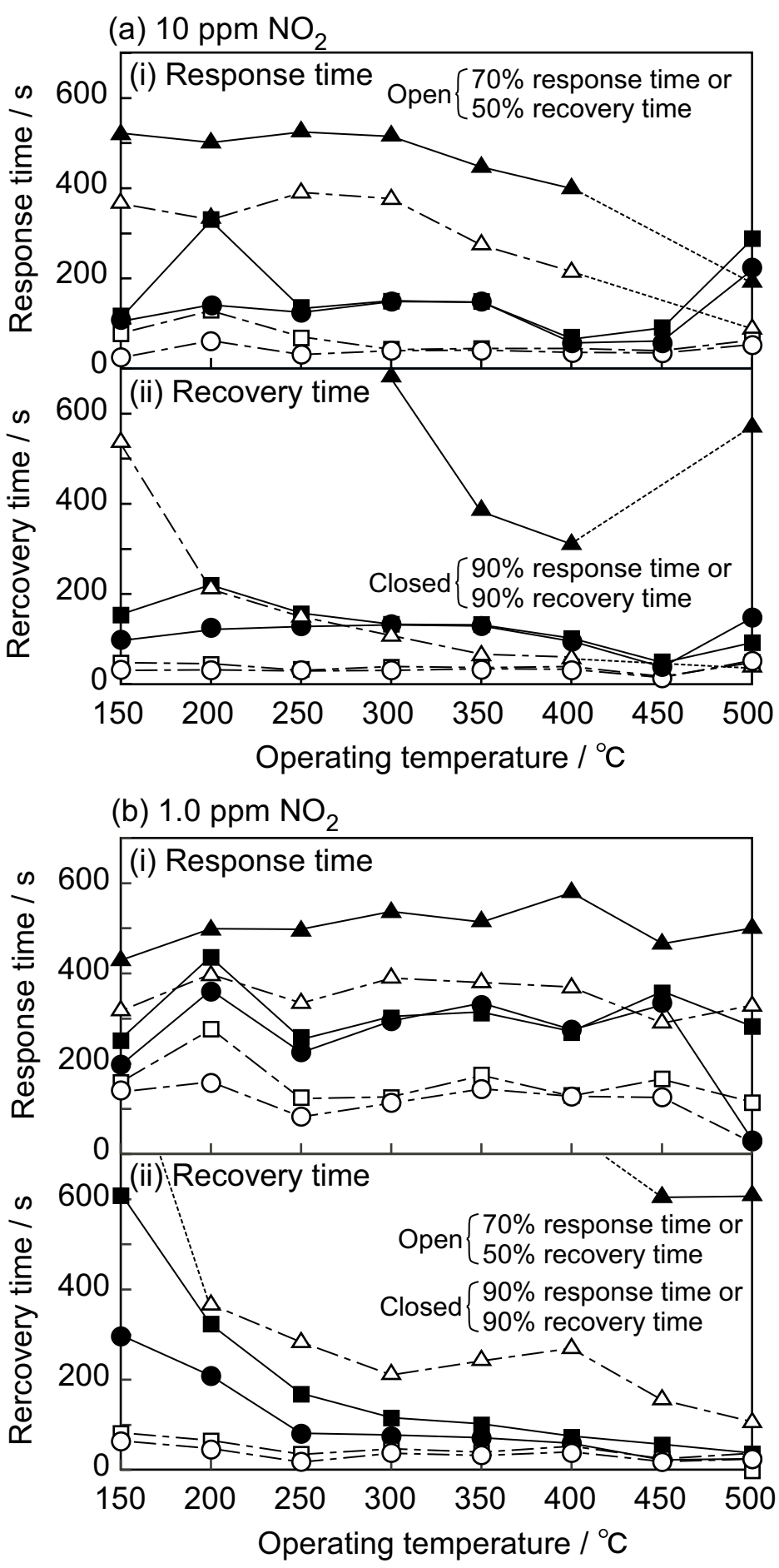

Fig. 14. Hyodo et al.